ARTICLE

Photovoltaic Performance of Triphenylamine Dyes-sensitized Solar Cells Employing Cobalt Redox Shuttle and Influence of π-conjugated Spacers

Jiang-nan Jia, Kai Tang, Mao Liang*, Hong-yu Han, Quan-ping Wu, Song Xue*

Department of Applied Chemistry, Tianjin University of Technology, Tianjin 300384, China

(Dated: Received on April 11, 2013; Accepted on May 16, 2013)

Developing photosensitizers suitable for the cobalt electrolyte and understanding the structure-property relationship of organic dyes is warranted for the dye-sensitized solar cells (DSSCs). The DSSCs incorporating tris(1,10-phenanthroline)cobalt(II/III)-based redox electrolyte and four synthesized organic dyes as photosensitizers are described. The photovoltaic performance of these dyes-sensitized solar cells employing the cobalt redox shuttle and the influences of the π-conjugated spacers of organic dyes upon the photovoltage and photocurrent of mesoscopic titania solar cells are investigated. It is found that organic dyes with thiophene derivates as linkers are suitable for DSSCs employing cobalt electrolytes. DSSCs sensitized with the as-synthesized dyes in combination with the cobalt redox shuttle yield an overall power conversion efficiency of 6.1% under 100 mW/cm^2 AM1.5 G illumination.

Key words: Dye-sensitized solar cell, Organic dye, Cobalt redox shuttle, Mass transport, Charge recombination

I. INTRODUCTION

Dye-sensitized solar cells (DSSCs) have received great attention because of their low cost and great potential in large-scale applications since reported by O'Regan and Grätzel in 1991 [1−3]. To date, the ruthenium-based dyes together with an iodide/triiodide redox couple system has afforded the best power conversion efficiencies of 11.4% [4−6]. However, some disadvantages of the iodide/triiodide redox couple limit the performance of DSSCs, such as (i) its relatively high overpotential for dye regeneration has led to a noticeable potential loss [7], (ii) the halogen bonding between iodine and some electron-rich segments of dye molecules could cause a larger charge recombination rate at the titania/electrolyte interface [8−10], (iii) competitive light absorption by the triiodide has led to a light harvesting loss [11, 12], (iv) the large-scale manufacturing of DSSCs remains a challenge due to the corrosiveness of the iodide/triiodide redox couple toward most metals and sealing materials [13, 14]. Thus, research on replacing the conventional iodide/triiodide electrolyte system in DSSCs with cobalt-complex based redox couples is at present receiving great attention [15].

Recent studies have shown that cobalt redox couples can give impressively high efficiencies comparable to iodide/triiodide electrolyte by using organic dyes. By employing a combination of an zinc porphyrin dye (YD2-o-C8) and an organic dye (Y123) in conjunction with tris(2,2′-bipyridine)cobalt(II/III) redox couple, Grätzel *et al.* showed a 12.3% of efficiency DSSC [15]. The efficiency exceeds those obtained with today's best ruthenium sensitizers. A cobalt complex using tridendate ligands $[Co(bpy\text{-}pz)_2]^{3+/2+}$ $(PF_6)_{3/2}$ as redox mediator in combination with a cyclopentadithiophene-bridged donor-acceptor dye (Y123), adsorbed on TiO_2, yielded a power conversion efficiency of over 10% at 100 mW/cm^2 [16]. Wang *et al.* explored the tris(1,10-phenanthroline)cobalt(II/III) redox shuttles in conjunction with the triphenylamine-based organic dyes to fabricate DSSCs displaying power conversion efficiency of 5.8%−9.4% [17−20]. Boschloo and Hagfeldt *et al.* reported triphenylamine-based organic dyes based DSSCs employing the tris(2,2′-bipyridine)cobalt(II/III) redox shuttles displaying the best efficiency of 6.7%. An advantage of the cobalt electrolytes over iodide/triiodide redox couple is that very high open-circuit voltage (V_{OC}) can be realized but without sacrificing short circuit photocurrent or fill factor [13]. However, simply replacing the iodide/triiodide couple in the DSSCs by cobalt redox couples may lead to poorly performing devices with low photovoltages [14, 21−24], indicating a different structure-property relationship of organic dyes in cobalt cells compared to those in iodine cells. Therefore, developing new photosensitizers suitable for DSSCs employing cobalt electrolytes is warranted. In addition, a comprehensive understanding on the structure-property relationship of organic dyes in cobalt cells will play a pivotal role in further development of iodine-free high-efficiency devices.

Herein, we report the performance of four dihexyloxy-

*Authors to whom correspondence should be addressed. E-mail: liangmao717@126.com, xuesong@ustc.edu.cn, Tel.: +86-22-60214250, FAX: +86-22-60214252

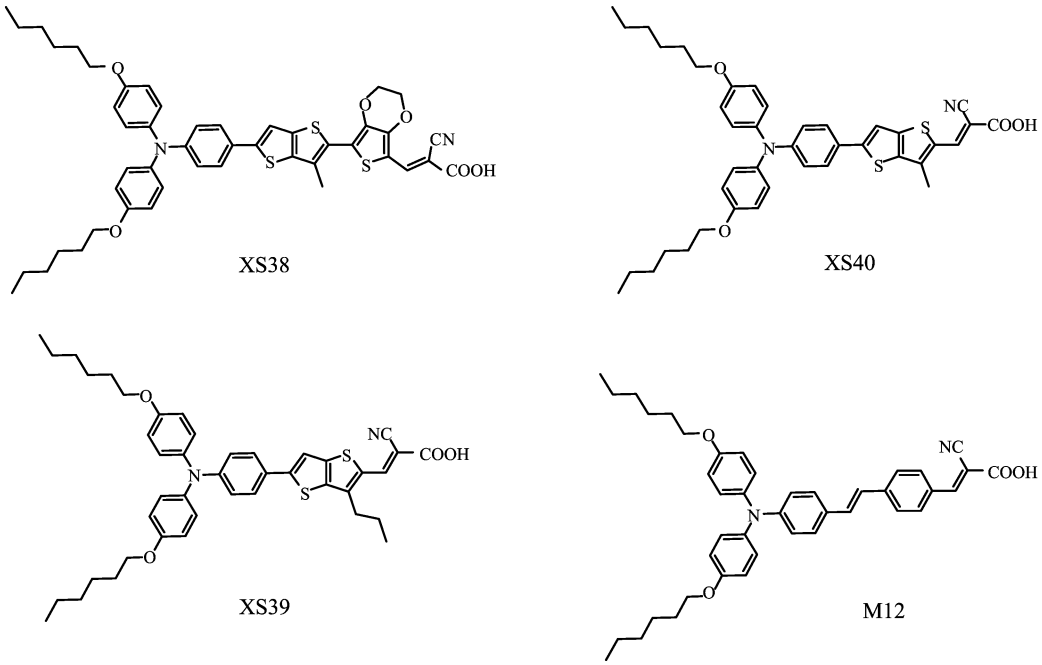

Scheme 1 Molecular structures of dyes.

substituted triphenylamine dyes-sensitized solar cells XS38−40 and M12 (Scheme 1) employing cobalt or iodine electrolytes. We also investigate the influences of π-conjugated spacer of organic dyes upon the photovoltage and photocurrent of mesoscopic titania solar cells, by employing the four dyes with alkyl-substituted thieno[3,2-b]thiophene, phenylene and combined 3,4-ethylenedioxythiophene (EDOT) and methyl-substituted thieno[3,2-b]thiophene as the π-conjugated spacers.

II. EXPERIMENTS

A. Materials and methods

The synthetic routes of the XS39 and XS40 are shown in Scheme 2. XS38 and M12 were prepared according to our previous work [25, 26]. *N*, *N*-Dimethylformamide was dried over and distilled from CaH_2 under an atmosphere of nitrogen. Titanium(IV) isopropoxide, tertbutylpyridine, 1,10-Phenanthroline (phen), $NOBF_4$, potassium hexafluorophosphate (KPF_6) and Lithium bis-(trifluoromethanesulfonyl)imide (LiTFSI) were purchased from J&K Scientific Ltd. All other solvents and chemicals used in this work were analytical grade and used without further purification.

Melting points of the samples were taken on an RY-1 melting point apparatus (Tianfen, China). ^{1}H NMR and ^{13}C NMR spectra were recorded on a Bruker AM-400 spectrometer. The reported chemical shifts were against TMS. High resolution mass spectra were obtained with a Micromass GCT-TOF mass spectrometer.

B. Detailed experimental procedures and characterization

1. 4-(hexyloxy)-N-(4-(hexyloxy)phenyl)-N-(4-(6-propylthieno [3,2-b]thiophen-2-yl)phenyl)benzenamine (compound **2**)

$Pd(PPh_3)_4$ (120 mg, 0.10 mmol) was placed to a 100 mL two-neck round-bottom flask, then air was extracted under vacuum and N_2 was introduced in. Compound **1** (1.00 g, 1.91 mmol) and tributyl(6-propylthieno[3,2-b]thiophen-2-yl)stannane (1.08 g, 2.29 mmol) was dissolved in 45 mL toluene. The mixture solution was added into the flask and heated to reflux. After 6 h, the result solution was cooled to room temperature. Water was added to quench the reaction, and the result mixture was extracted with CH_2Cl_2 (DCM). The combined organic layer was dried over anhydrous magnesium sulfate, then concentrated under vacuum. The residue was applied onto a silica gel column with DCM/PE (1:5) and resulted in 561 mg (47%) yellow green oil. ^{1}H NMR (400 MHz, $CDCl_3$): δ 7.53−7.31 (m, 3H), 7.20−6.97 (m, 4H), 6.97−6.68 (m, 7H), 4.08−3.84 (m, 4H) 2.71 (t, J=8.0 Hz, 2H), 1.84−1.74 (m, 6H), 1.52−1.43 (m, 4H), 1.40−1.32 (m, 8H). 1.01 (t, J=7.3 Hz, 3H), 0.95−0.89 (m, 6H). ^{13}C NMR (100 MHz, $CDCl_3$): δ 155.8, 148.6, 146.2, 140.5, 139.5, 138.2, 135.1, 126.9, 126.5, 120.8, 120.4, 115.5, 114.4, 68.4, 32.2, 31.8, 29.5, 25.9, 22.8, 22.1, 14.2, 14.1. HRMS (ESI) calcd. for $C_{39}H_{47}NO_2S_2$ ($M+H^+$): 626.3126. Found: 626.3129.

DOI:10.1063/1674-0068/26/03/310-320

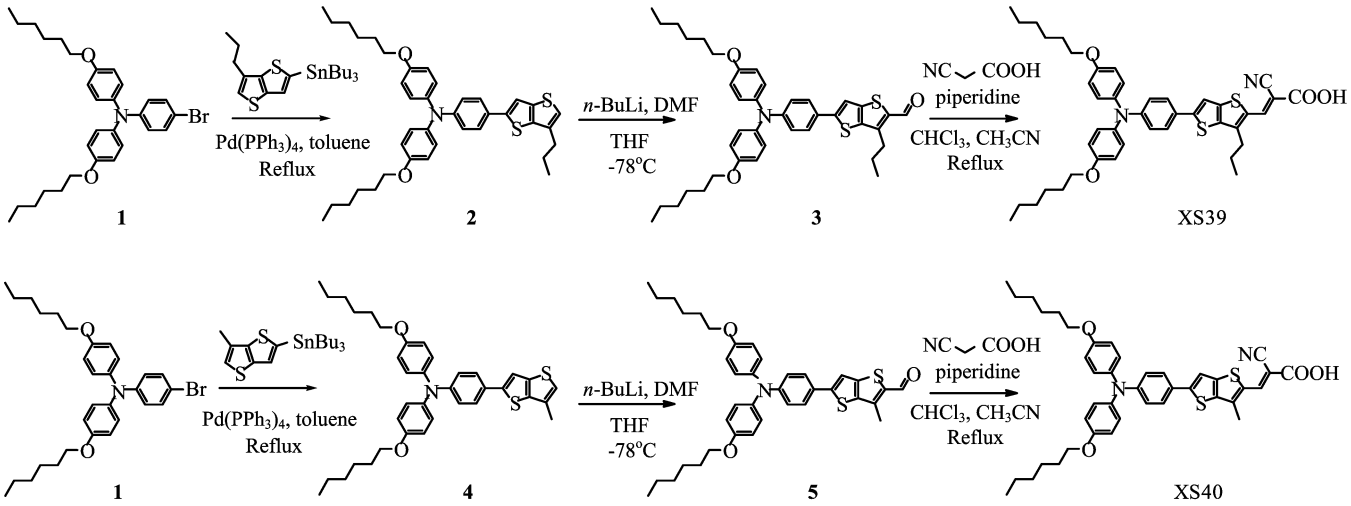

Scheme 2 Synthetic route to XS39 and XS40.

2. 5-(4-(bis(4-(hexyloxy)phenyl)amino)phenyl)-3-propyl thieno[3,2-b]thiophene-2-carbaldehyde (compound **3**)

Compound **2** (318 mg, 0.51 mmol) was dissolved in 50 mL of THF into a 100 mL two-neck round-bottom flask. The solution was cooled to −78 °C and *n*-BuLi (0.32 mL, 0.76 mmol) was added dropwise slowly. After stirring for 1 h, DMF (0.047 mL, 0.61 mmol) was added at −78 °C. Then, the reaction was warmed to room temperature smoothly overnight. Water was added to quench the reaction, and the result mixture was extracted with DCM. The combined organic layer was dried over anhydrous magnesium sulfate, then concentrated under vacuum. The residue was applied onto a silica gel column with EA/PE (1:10) and resulted in 253 mg (76%) brown oil. ^{1}H NMR (400 MHz, $CDCl_3$): δ 10.04 (s, 1H), 7.42 (d, J=8.7 Hz, 2H), 7.32 (s, 1H), 7.09 (d, J=8.8 Hz, 4H), 6.92 (d, J=8.7 Hz, 2H), 6.85 (d, J=8.8 Hz, 4H), 3.93 (*t*, J=6.5 Hz, 4H), 3.06 (t, J=7.4 Hz, 2H), 1.91−1.82 (m, 2H), 1.80−1.75 (m, 4H), 1.49−1.43 (m, 4H), 1.37−1.32 (m, 8H), 1.02 (t, J=7.3 Hz, 3H), 0.93−0.89 (m, 6H). ^{13}C NMR (100 MHz, $CDCl_3$): δ 182.1, 156.2, 152.9, 149.8, 146.1, 145.1, 140.0, 139.1, 138.0, 127.3, 126.9, 119.5, 115.5, 114.3, 68.4, 31.7, 30.3, 25.9, 23.4, 22.7, 19.3, 14.2, 14.1. HRMS (ESI) calcd. for $C_{40}H_{47}NO_3S_2$ (M+H$^+$): 654.3075. Found: 654.3069.

3. 3-(5-(4-(bis(4-(hexyloxy)phenyl)amino)phenyl)-3-propyl thieno[3,2-b]thiophen-2-yl)-2-cyanoacrylic acid (XS39)

Compound **3** (100 mg, 0.53 mmol) was dissolved in acetonitrile (5 mL) and chloroform (2.5 mL) in a 25 mL round-bottom flask. Then cyanoacetic acid (20 mg, 0.24 mmol) and piperidine (100 μL) was added. The solution was heated to reflux. After stirring for 5 h, water was added to quench the reaction, and the result mixture was extracted with DCM. The organic layers combined and dried over anhydrous magnesium sulfate, then concentrated under vacuum. The residue was applied onto a silica gel column with DCM/MeOH (10:1) and resulted in 93 mg (88%) red powder. M.p=45−147 °C, ^{1}H NMR (400 MHz, DMSO-d_6): δ 8.27 (s, 1H), 7.79 (s, 1H), 7.55 (d, J=8.0 Hz, 2H), 7.08 (d, J=7.8 Hz, 4H), 6.94 (d, J=7.8 Hz, 4H), 6.77 (d, J=8.0 Hz, 2H), 3.94 (t, J=7.3 Hz, 3H), 2.88 (t, J=6.3 Hz, 2H), 1.76−1.65 (m, 6H), 1.47−1.36 (m, 4H), 1.36−1.26 (m, 8H), 0.96−0.84 (m, 9H). ^{13}C-NMR (100 MHz, DMSO-d6): δ 164.4, 149.1, 143.7, 139.0, 137.9, 131.3, 127.3, 126.7, 124.3, 118.3, 115.5, 114.9, 86.4, 67.6, 31.0, 29.9, 28.7, 25.2, 22.7, 22.1, 13.9, 13.8. HRMS (ESI) calcd. for $C_{43}H_{48}N_2O_4S_2$ (M+H$^+$): 721.3133. Found: 721.3141.

4. 4-(hexyloxy)-N-(4-(hexyloxy)phenyl)-N-(4-(6-methylthieno [3,2-b]thiophen-2-yl)phenyl)benzenamine (compound **4**)

The product was synthesized according to the procedure for the synthesis of compound **2**, giving a yellow oil in 41% yield. ^{1}H NMR (400 MHz, $CDCl_3$): δ 7.48−7.28 (m, 3H), 7.19−6.99 (m, 4H), 6.99−6.75 (m, 7H), 3.94 (m, 4H), 2.37 (s, 3H), 1.83−1.74 (m, 4H), 1.52−1.43 (m, 4H), 1.39−1.32 (m, 8H), 0.95−0.91 (m, 6H). ^{13}C NMR (100 MHz, $CDCl_3$): δ 155.8, 148.7, 146.4, 140.5, 139.4, 139.1, 130.0, 126.9, 126.5, 121.3, 120.4, 120.4, 115.5, 114.6, 68.4, 31.8, 29.5, 25.9, 22.8, 14.2, 13.7. HRMS (ESI) calcd for $C_{37}H_{43}NO_2S_2$ (M+H$^+$): 598.2813. Found: 598.2820.

5. 5-(4-(bis(4-(hexyloxy)phenyl)amino)phenyl)-3-methyl thieno[3,2-b]thiophene-2-carbaldehyde (compound **5**)

The product was synthesized according to the procedure for the synthesis of compound **3**, giving an or-

DOI:10.1063/1674-0068/26/03/310-320

ange oil in 80% yield. ^{1}H NMR (400 MHz, $CDCl_3$): δ 10.05 (s, 1H), 7.44 (d, J=8.7 Hz, 2H), 7.34 (s, 1H), 7.09 (d, J=8.8 Hz, 4H), 6.92 (d, J=8.7 Hz, 2H), 6.86 (d, J=8.8 Hz), 3.94 (t, J=6.5 Hz, 4H), 2.68 (s, 3H), 1.83−1.74 (m, 4H), 1.51−1.43 (m, 4H), 1.39−1.31 (m, 8H), 0.93−0.90 (m, 6H). ^{13}C NMR (100 MHz, $CDCl_3$): δ 182.2, 156.2, 153.0, 149.8, 145.7, 140.0, 139.9, 137.6, 127.3, 127.0, 125.2, 119.5, 115.5, 114.4, 68.4, 31.7, 29.4, 25.9, 22.8, 14.2, 13.7. HRMS (ESI) calcd for $C_{38}H_{43}NO_3S_2$ ($M+H^+$): 626.2762. Found: 626.2755.

6. 3-(5-(4-(bis(4-(hexyloxy)phenyl)amino)phenyl)-3-methyl thieno[3,2-b]thiophen-2-yl)-2-cyanoacrylic acid (XS40)

The product was synthesized according to the procedure for the synthesis of XS39, giving a red powder in 85% yield. M.p=132−134 °C, ^{1}H NMR (400 MHz, DMSO-d_6): δ 8.35 (s, 1H), 7.83 (s, 1H), 7.57 (d, J=8.6 Hz, 2H), 7.09 (d, J=8.6 Hz, 4H), 6.94 (d, J=8.6 Hz, 4H), 6.77 (d, J=8.6, 2H), 3.94 (t, J=6.3 Hz, 4H), 2.53 (s, 3H), 1.74−1.67 (m, 4H), 1.44−1.38 (m, 4H), 1.34−1.29 (m, 8H), 0.91−0.86 (m, 6H). ^{13}C NMR (100 MHz, DMSO-d_6): δ 164.1, 155.8, 152.0, 149.3, 144.8, 143.4, 139.0, 138.7, 130.7, 127.3, 126.8, 124.1, 118.2, 117.2, 115.5, 115.0, 87.5, 67.6, 31.0, 28.7, 25.2, 22.1, 13.9, 13.8. HRMS (ESI) calcd for $C_{41}H_{44}N_2O_4S_2$ ($M+H^+$): 693.2820. Found: 693.2826.

C. Photophysical and electrochemical measurements

The absorption spectra of the dyes-sensitized TiO_2 films were measured by JASCO-V550 spectrophotometer. Adsorption of the dye on the TiO_2 surface was done by soaking the TiO_2 electrode in a mixture solution ethanol-dichloromethane (3:1, volume ratio) solution of the dye (standard concentration 3×10^{-4} mol/L) at room temperature for 24 h.

Cyclic voltammetry measurements were performed at room temperature on a computer controlled LK2005A electrochemical workstation with Pt-wires as working electrode and counter electrode, Ag/AgCl electrode as reference electrode at a scan rate of 100 mV/s. Tetrabutylammonium perchlorate (TBAP, 0.1 mol/L) and MeCN were used as supporting electrolyte and solvent, respectively. The measurements were calibrated using ferrocene as standard. The redox potential of ferrocene (F_c) internal reference is taken as 0.63 V *vs.* NHE [25].

Electrochemical impedance spectroscopy (EIS) in the frequency range of 100 mHz to 100 kHz was performed with a PARSTAT 2273 potentiostat/galvanostat/FRA in the dark with the alternate current amplitude set at 10 mV.

D. Fabrication of DSSCs

TiO_2 colloid was prepared according to the literature method [27], which was used for the preparation of the nanocrystalline films. The TiO_2 paste consisting of 18% TiO_2, 9% ethyl cellulose and 73% terpineol was firstly prepared, which was printed on a conducting glass (Nippon Sheet Glass, Hyogo, Japan, fluorine-doped SnO_2 over layer, sheet resistance of 10 Ω/sq) using a screen printing technique. The thickness of the TiO_2 film was controlled by selection of screen mesh size and repetition of printing. The film was dried in air at 120 °C for 30 min and calcined at 500 °C for 30 min under flowing oxygen before cooling to room temperature. The heated electrodes were impregnated with a 0.05 mol/L titanium tetrachloride solution in a water-saturated desiccator at 70 °C for 30 min and fired again to give a ca. 5.5 μm thick mesoscopic TiO_2 film. The TiO_2 electrode was stained by immersing it into a dye solution containing 300 μmol/L dye sensitizers (ethanol-dichloromethane 3:1) for 24 h at room temperature. Then the sensitized-electrode was rinsed with dry ethanol and dried by a dry air flow. Pt catalyst was deposited on the FTO glass by coating with a drop of H_2PtCl_6 solution (40 mmol/L in ethanol) with the heat treatment at 395 °C for 15 min to give photoanode. The dye-covered TiO_2 electrode and Pt-counter electrode were assembled into a sandwich type cell according to the literature method [27]. The dye-covered TiO_2 electrode and Pt-counter electrode were assembled into a sandwich type cell by a 25 μm-thick Surlyn (DuPont) hot-melt gasket and sealed up by heating. The cobalt electrolyte, CM22, is composed of 0.25 mol/L $[Co(II)(phen)_3](PF_6)_2$ [14], 0.05 mol/L $[Co(III)(phen)_3](PF_6)_3$, 0.5 mol/L 4-tertpyridine (TBP) and 0.1 mol/L LiTFSI in acetonitrile. For comparison, an iodine electrolyte consisting of 0.25 mol/L 1,2-dimethyl-3-*n*-propylimidazolium iodide (DMPImI), 0.1 mol/L LiTFSI, 0.05 mol/L I_2, and 0.5 mol/L tertbutylpyridine in acetonitrile, namely CM24, was formulated.

E. Characterization of DSSCs

The photocurrent-voltage (J-V) characteristics of the solar cells were carried out using a Keithley 2400 digital source meter controlled by a computer and a standard AM1.5 solar simulator-Oriel 91160-1000 (300W) SOLAR SIMULATOR 2×2 BEAM. The light intensity was calibrated by an Oriel reference solar cell. A metal mask with an aperture area of 0.16 cm^2 was covered on a testing cell during all measurements. The action spectra of monochromatic incident photon-to-current conversion efficiency (IPCE) for solar cell were performed by using a commercial setup (QTest Station 2000 IPCE Measurement System, CROWNTECH, USA).

III. RESULTS AND DISCUSSION

A. UV-Vis absorption

The absorption and emission spectra of XS39 and XS40 in dichloromethane are shown in Fig.1(a). Ow-

DOI:10.1063/1674-0068/26/03/310-320

TABLE I Optical properties and electrochemical properties of the dyes.

Dye	λ_{max}/nm (ε^a/10^3(mol/L)$^{-1}$cm^{-1})	$\lambda_{int}{}^b$/nm	$E_{0-0}{}^c$/eV	$E(S/S^+)^d$/V (*vs.* NHE)	$E(S^*/S^+)^e$/V (*vs.* NHE)
XS38	494 (37)	574	2.16	0.83	−1.43
XS39	474 (33)	565	2.19	0.82	−1.36
XS40	477 (35)	593	2.09	0.82	−1.26
M12	453 (14)	537	2.31	0.83	−1.48

[a] Absorption peaks of dyes measured in CH_2Cl_2, ε is the extinction coefficient at λ_{max} of absorption.
[b] The intersect of the normalized absorption and the emission spectra.
[c] E_{0-0} values were estimated from the intersections of normalized absorption and emission spectra (λ_{int}): E_{0-0}=1240/λ_{int}.
[d] $E(S/S^+)$ was recoded by cyclic voltammograms of the dye-loaded TiO_2 film.
[e] $E(S^*/S^+)$ was calculated from $E(S/S^+)-E_{0-0}$.

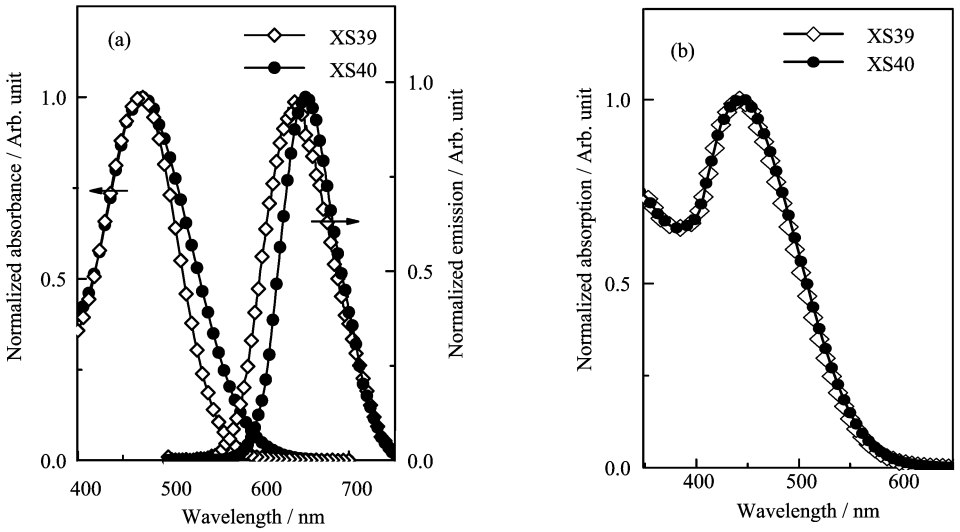

FIG. 1 (a) Absorpiton/emission spectra of XS39 and XS40 in DCM and (b) absorption spectra of dyes-sensitized TiO_2 film (3 μm).

ing to their similar structure, XS39 and XS40 exhibit similar intramolecular charge-transfer transition (ICT) electron transition peaks located in the range of 400−600 nm. The values of molar extinction coefficient, ε, at the maximum absorption wavelength, λ_{max}, for XS39 and XS40 are 3.3×10^4 and 3.5×10^4 (mol/L)$^{-1}$cm^{-1}, respectively. Under the same conditions, M12 shows a blue-shifted absorption relative to XS39 and XS40 together with decreasing the molar extinction coefficient (ε=1.4×10^4 (mol/L)$^{-1}$cm^{-1} at 453 nm) [25]. The red-shifted spectral response and higher molar absorption coefficient of XS39 and XS40 can be caused by a stronger electron-rich thieno[3,2-b]thiophene unit related to phenylene, which is desirable for light harvesting and thin-film using. In contrast, XS38 exhibits a red-shifted spectral response compared to those of XS39 and XS40 (Table I) due to extension of the linker conjugation. Upon adsorption onto transparent mesoporous TiO_2 films (3 μm), XS39 and XS40 show an evident hypsochromic effect compared with that measured in solution (Fig.1(b)), indicating a weaker electron-withdrawing capability of

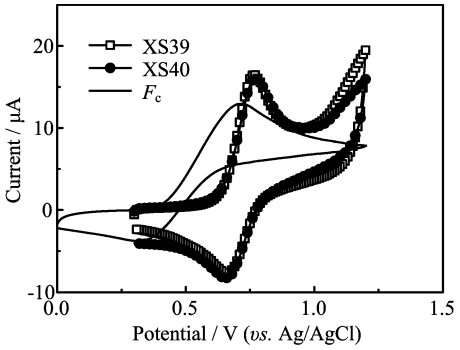

FIG. 2 Cyclic voltammogram of XS38−40 and F_c.

the carboxylatetitanium assembly than that of the carboxylic acid. Emission maxima of dyes XS39-40 can be found at 500−700 nm when the dyes are excited at their respective absorption bands at 400−500 nm (Table I).

The ground-state oxidation potential ($E(S/S^+)$) of XS39 and XS40 in MeCN were determined from cyclic voltammogram (Fig.2). The optical and the electro-

DOI:10.1063/1674-0068/26/03/310-320

TABLE II Photovoltaic performance of DSSCs using a 5.5 μm film. The parameters include short-circuit photocurrent density (J_{SC}), open-circuit photovoltage (V_{OC}), fill factor (F_F), and power conversion efficiency (PCE). Cobalt: 0.25 mol/L $[Co(II)(phen)_3](PF_6)_2$, 0.05 mol/L $[Co(III)(phen)_3](PF_6)_3$, 0.5 mol/L TBP and 0.1 mol/L LiTFSI in acetonitrile. Iodide: 0.25 mol/L DMPImI, 0.1 mol/L LiTFSI, 0.05 mol/L I_2, and 0.5 mol/L TBP in acetonitrile.

Dye	J_{SC}/(mA/cm^2)	V_{OC}/mV	F_F	PCE/%	Dye load /(mol/cm^2)
XS38/Cobalt	8.6	810	0.69	4.8	2.0×10^{-7}
XS38/Iodine	10.5	700	0.68	5.0	
XS39/Cobalt	9.7	846	0.71	5.8	2.7×10^{-7}
XS39/Iodine	10.7	730	0.68	5.3	
XS40/Cobalt	10.2	842	0.71	6.1	3.1×10^{-7}
XS40/Iodine	11.3	725	0.68	5.6	
M12/Cobalt	7.9	795	0.69	4.3	2.5×10^{-7}
M12/Iodine	10.2	756	0.68	5.2	

chemical data of the four dyes have been presented in Table I. In the iodine control cells, the driving forces for dye regeneration of XS38-40 and M12 are more positive than the iodine redox potential (0.4 V *vs.* NHE [11]). Thus, the oxidized dyes could be regenerated from the reduced species in the electrolyte to give an efficient charge separation. In the cobalt control cells, the driving forces for dye regeneration of the dyes are 0.2−0.21 eV compared to the redox potential of $[Co(II/III)(phen)_3]^{n+}$ (0.62 V *vs.* NHE [14]). Recently, Wenger *et al.* prove that efficient regeneration of sensitizers with as little as a 0.15 eV driving force is possible [28]. Therefore, the low driving force of XS38−40 and M12 for regeneration can be used to increase the voltage of DSSCs. On the other hand, the excited-state reduction potential ($E(S^*/S^+)$) of XS38−40 and M12 (−1.26 V to −1.48 V *vs.* NHE, respectively) is more negative than the conduction band of TiO_2 (−0.5 V *vs.* NHE [29]). Assuming that energy gap of 0.2 eV is necessary for efficient electron injection [30], these driving forces are sufficiently large for effective electron injection.

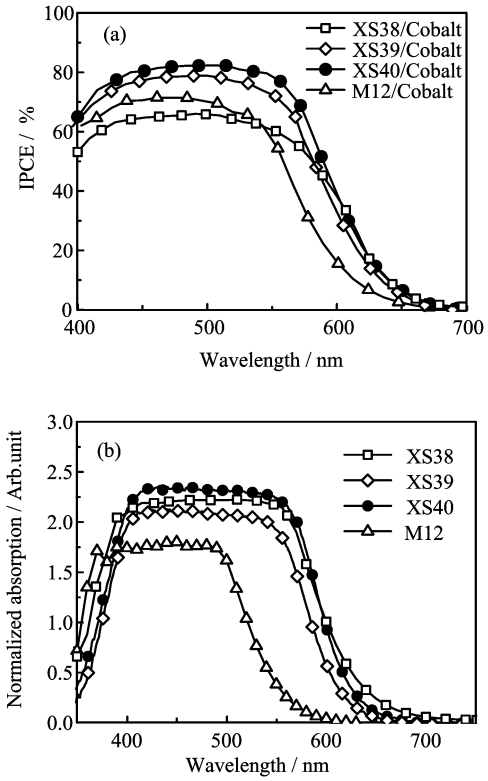

FIG. 3 (a) IPCEs action spectra of devices and (b) absorption spectra of dyes-sensitized TiO_2 film (5.5 μm).

B. Photovoltaic performance of DSSCs

Using the four dyes as sensitizers, we compared the photovoltaic performance of DSSCs employing a cobalt electrolyte (CM22) with those employing an iodine electrolyte (CM24). A relatively thin titania film (5.5 μm) is employed so as to avoid the mass transport limitation of tris(phen)cobalt(II/III) redox couple and to minimize interfacial charge recombination. The incident-photon-to-current conversion efficiency (IPCE) for DSSCs sensitized with the four dyes employing the cobalt electrolyte using a 5.5 μm single-layer TiO_2 film is shown in Fig.3(a). IPCE with more than 70% values are observed in the range of 430−580 nm for XS39- and XS40-sensitized devices. XS40-sensitized device generates the highest short-circuit photocurrent density (J_{SC}) among the four sensitizers (Table II), which can be attributed to its broad and intense photocurrent action spectrum. It also noted that the IPCE performance of XS40-sensitized device is higher than that of XS39, probably due to the stronger π-π interaction in XS40 than that in XS39 because the longer alkyl chain can weaken the π-π interaction. As presented in Fig.3(b), the absorption intensity of XS39 loaded TiO_2 film is slightly lower than that of XS40. By comparing the absorbance change of a dye solution (300 μmol/L) before and after dye up-taking with a titania film, the surface coverages (Γ) of XS39 and XS40 anchored on TiO_2 film were de-

DOI:10.1063/1674-0068/26/03/310-320

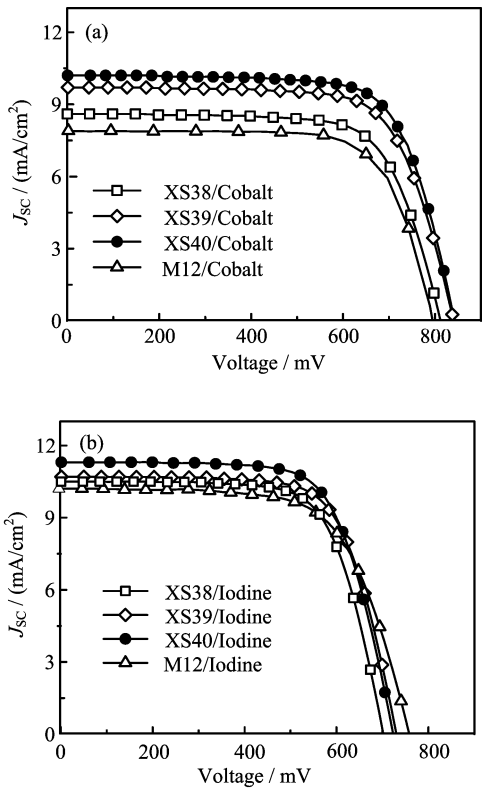

FIG. 4 *J-V* characteristics of DSSCs employing (a) the cobalt electrolyte and (b) the iodide electrolyte.

termined to be 2.7×10^{-7} and 3.1×10^{-7} mol/cm^2, respectively. Obviously, the lower dye adsorption amount for XS39 on TiO_2 surface stems from the larger molecular size and weaker intermolecular π-π interaction. XS38-sensitized device shows a broad IPCE in accordance with the broad absorption spectrum achieved by introduction of binary spacers of EDOT and methyl-substituted thieno[3,2-b]thiophene. In agreement with the trend in absorption spectra of dye-sensitized film (Fig.3(b)), the IPCE spectra of M12-sensitized device exhibits a narrower IPCE spectrum related to those of the XS38-XS40, leading to a relatively lower J_{SC} of 8.6 mA/cm^2 (Table II).

The photocurrent density-voltage (*J-V*) curves of the devices measured under AM 1.5 irradiation (100 mW/cm^2) are shown in Fig.4 and the detailed photovoltaic parameters are summarized in Table II. The short-circuit photocurrent density (J_{SC}), open-circuit photovoltage (V_{OC}), and fill factor (F_F) of a XS40-sensitized cell with the cobalt electrolyte are 10.2 mA/cm^2, 842 mV, and 0.71, respectively, affording an overall power conversion efficiency (PCE) of 6.1%. In contrast, the XS40-sensitized device with the iodide electrolyte exhibits a slightly increased J_{SC} of 11.3 mA/cm^2 and a remarkably decreased V_{OC} of 725 mV, leading to a relatively lower PCE of 5.6%. The XS39-sensitized device, when combined with the cobalt electrolyte, also generates remarkably improved V_{OC}, resulting in an enhanced PCE of 5.8%. Evidently, XS40 is better in terms of solar cell performance, especially in J_{SC}, which is in agreement with the observed IPCEs. These results confirm that for XS39 and XS40, the tris(phen)cobalt(II/III) redox couple outperforms the I^-/I_3^- redox couple for thin-film DSSCs. In contrast, M12- and XS38-sensitized devices exhibit better performance when employing the iodine electrolyte.

C. TiO_2 surface interfacial charge recombination in cobalt cells

Electrochemical impedance spectroscopy (EIS) is a powerful tool for identifying electronic and ionic transport processes in DSSCs, which provides valuable information for the understanding of photovoltaic parameters (J_{SC}, V_{OC}, F_F and η). Figure 5 shows the typical EIS Nyquist and Bode phase plots of the cobalt cells measured under the dark conditions at a forward bias of -0.75 V. The equivalent circuit [31] presented in Fig.5(b) was used to fit the experimental data of all of the samples. R_s is the series resistance accounting for the transport resistance of the TCO and the electrolyte. C_μ and R_{CT} are the chemical capacitance and the charge recombination resistance at the TiO_2/electrolyte interface, respectively. C_{Pt} and R_{Pt} are the interfacial capacitance and charge transport resistance at the Pt/electrolyte interface, respectively. The larger semicircle at lower frequencies represents the interfacial R_{CT} at the TiO_2/dye/electrolyte interface. The fitted R_{CT} increases in the order of M12 (338 Ω)<XS38 (825 Ω) <XS39 (1320 Ω), which is consistent with the sequence of V_{OC} values in the devices. The smaller R_{CT} value means the electron recombination from the conduction band to the electrolyte occurring more easily, and thus results in lower V_{OC}. Clearly, electron recombination in cobalt cells based on M12 is faster than that of XS38 and XS39.

D. Dependence of photovoltage on the conduction band movement and charge recombination

It is noteworthy that the dye alteration in the iodine cells from M12 to XS38/XS39 has caused a V_{OC} attenuation of 56/26 mV, sharply contrasting a 15/51 mV enhancement in the cobalt cells. The V_{OC} values are in the sequence of XS38<XS39<M12 for the iodine cells, while in the sequence of M12<XS38<XS39 for the cobalt cells. The opposite V_{OC} variation for the iodine and cobalt cells in the case of sensitizer change from M12 to XS38/XS39 is intriguing. To scrutinize the origin of the improvement in V_{OC}, possible factors influencing V_{OC} for DSSCs based on the three dyes involving the conduction band (E_{CB}) movement and the free electron density (n_c) in TiO_2 will be discussed in detail in the following sections.

DOI:10.1063/1674-0068/26/03/310-320

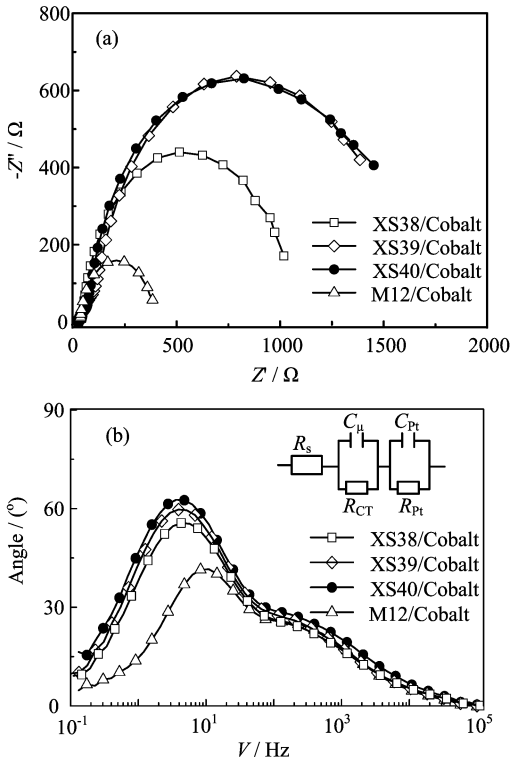

FIG. 5 (a) Nyquist plots and (b) Bode phase plots of electrochemical impedance spectra for the DSSCs based on XS38-XS40 and M12. The inset is the equivalent circuit used to fit the impedance spectra. R_s is the series resistance accounting for the transport resistance of the TCO and the electrolyte. C_μ and R_{CT} are the chemical capacitance and the charge recombination resistance at the TiO_2/electrolyte interface, respectively. C_{Pt} and R_{Pt} are the interfacial capacitance and charge transport resistance at the Pt/electrolyte interface, respectively.

The value of V_{OC} is determined by the potential difference between the Fermi-level of TiO_2 ($E_{F,n}$) and the Fermi-level of a redox electrolyte ($E_{F,redox}$), which could be described as Eq.(1) [32]

$$V_{OC} = E_{F,redox} - E_{F,n} \quad (1)$$

On the other hand, the $E_{F,n}$ of TiO_2 can be expressed as

$$E_{F,n} = E_{CB} + k_B T \ln\left(\frac{n_c}{N_c}\right) \quad (2)$$

where k_B is the Boltzmann constant, T is the temperature (293 K in this work), n_c is the free electron density, and N_c is the density of accessible states in the conduction band [18]. Considering that $E_{F,redox}$ would not change strongly in DSSCs with a fixed redox electrolyte, V_{OC} is intimately correlated to the E_{CB} and n_c. The $E_{F,n}$ levels can be calculated from the $E_{F,redox}$ and V_{OC} according to Eq.(1). As presented in Fig.6, the $E_{F,n}$ levels of XS38, XS39, and M12 are −0.19, −0.226, and −0.175 V, respectively, taken the $E_{F,redox}$ of $Co(II)(phen)_3(PF_6)_2$ as 0.62 V *vs.* NHE.

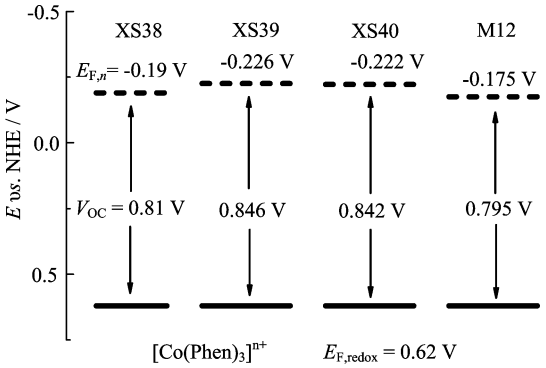

FIG. 6 The $E_{F,n}$ positions of DSSCs with the cobalt electrolyte.

To investigate the influences of the shift in the TiO_2 CB and charge recombination on $E_{F,n}$, impedance spectra were also measured by varying the applied potential at equal intervals in the vicinity of V_{OC}. The measured impedance spectra were fitted with the ZSimpWin (v 3.10) in terms of an equivalent circuit adaptable to DSSCs [33]. The chemical capacitance (C_μ) of cells can be expressed as an exponential function of potential bias, which are shown in Fig.7. This exponential rise with the increase of forward bias is a behavior of typical C_μ that is described by Eq.(3) [34, 35]

$$C_\mu = \frac{e^2}{k_B T} \exp\left[\frac{\alpha}{k_B T}\left(E_{F,redox} + eV_a - E_{CB}\right)\right] \quad (3)$$

where e is elementary charge, α is a constant related to the distribution of electronic states below the conduction. Considering that $E_{F,redox}$ would not change strongly in DSSCs fabricated under similar conditions [36], therefore, the C_μ is governed by the applied potential (V_a) and E_{CB}.

For the cobalt cells, at a given value of V_a, the C_μ for these dyes are in the order M12>XS38>XS39 (Fig.7(a)), indicating a sequential positive shift of the E_{CB} [37]. Generally, positive shift of E_{CB} leads to an open-circuit photovoltage loss for DSSCs. The sequence of conduction band movement is consistent with the sequence of V_{OC} values in the devices employing the cobalt electrolyte, indicating that the movement E_{CB} for the cobalt cells is partially responsible for the variation of V_{OC}. For the iodine cells (Fig.7(b)), the sequential of conduction band edge shifts for XS39 *vs.* M12 is in accordance with that of V_{OC} but not for XS38 *vs.* XS39. The increased V_{OC} is mainly ascribed to the increase in R_{CT} for XS39 compared to XS38.

The charge recombination resistance at the TiO_2/electrolyte interface (R_{CT}) was further modeled from impedance spectroscopies as a function of $E_{F,n}$ level (Fig.8). The charge recombination resistance is related to the charge recombination rate, such that a

DOI:10.1063/1674-0068/26/03/310-320

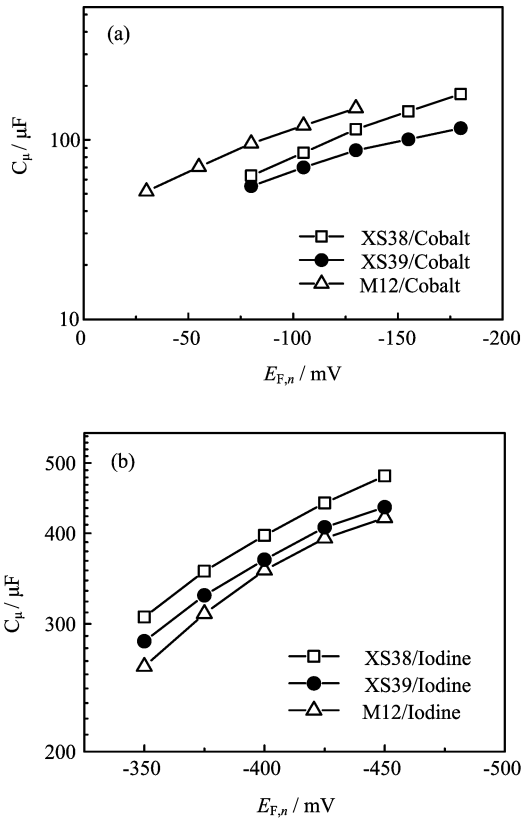

FIG. 7 Plots of chemical capacitance versus potential bias of (a) the cobalt cells and (b) the iodine cells.

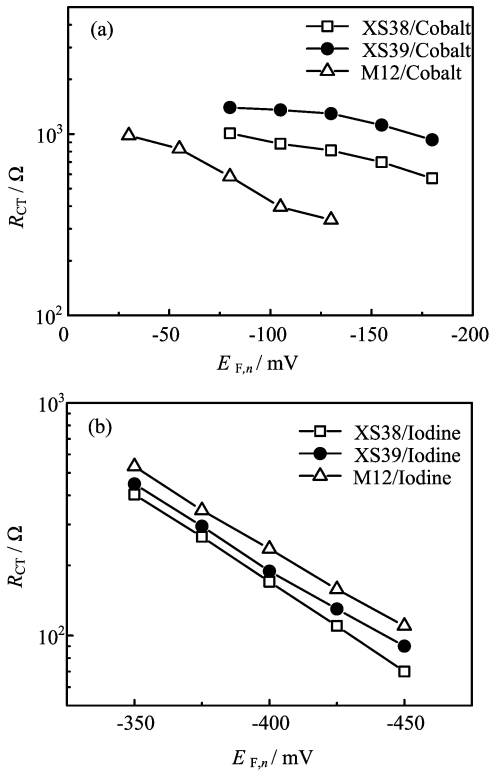

FIG. 8 Plots of R_{CT} *vs.* $E_{F,n}$ level of (a) the cobalt cells and (b) the iodine cells.

smaller R_{CT} means the larger charge recombination rate. As presented in Fig.8(a), for the cobalt cells, the fitted R_{CT} increases in the order of M12<XS38<XS39, indicating the same order of decreased charge recombination rate. On the other hand, the cobalt-to-iodine electrolyte alteration has caused a contrary consequence: the fitted R_{CT} increases in the order of XS38<XS39<M12. It is noted that, the sequence of R_{CT} values is consistent with the sequence of V_{OC} values in the devices employing iodine electrolyte, implying that it is charge recombination, rather than the position of CB, that governs V_{OC}.

We suspect that the R_{CT} variation of the three dyes in different electrolytes is probably due to the following reasons: it is known that the halogen bonding between iodine and some electron-rich segments of dye molecules could cause a larger charge recombination rate at the titania/electrolyte interface [8, 10, 37, 38]. Therefore, the R_{CT} variation of the dyes in different electrolytes is probably related to the adverse impact of possible halogen bonding on interfacial charge recombination in DSSCs. XS38 and XS39 containing methyl-substituted thieno[3,2-b]thiophene and EDOT with more interaction sites (sulfur atom) prefers formation of dye-iodine complexes in comparison with M12. Thereby, the increasing I_3^- concentration at the vicinity of the TiO_2 decreases the electron lifetimes, leading to a lower R_{CT} for XS38 and XS39-sensitized devices. Apart from the adverse impact of possible halogen bonding, the linker length also has an important impact on the surface blocking effect of dyes, which is correlated to the R_{CT} values. Recent studies have shown that the surface blocking of the dye layer as well as the electron lifetime would suffer from an extension of the linker conjugation [9]. Clearly, XS38 showed enhanced electron recombination in comparison to XS39 when used in the iodine cells due to the cumulative adverse effects arising from the possible halogen bonding and extension of the linker conjugation. In cobalt cells, higher R_{CT} of XS39-sensitized device related to that of M12 can be partially ascribed to the absence of this non-covalent interaction between the dyes and electrolytes. These results provide a new clue to understand the halogen-bonding issue in DSSCs, suggesting that organic dyes with thiophene derivates as linkers are suitable for DSSCs employing cobalt electrolytes.

We further compare the dependencies of R_{CT} on the $E_{F,n}$ level for cells with the cobalt and iodine electrolytes. It can be found from Fig.8 that, compared to the iodine cells, the employment of the cobalt electrolyte brings forth smaller R_{CT}, *i.e.*, an acceleration of charge recombination at the titania/electrolyte interface, leading to shorter electron lifetime. This adverse impact of a shorter electron lifetimes upon photovoltage partially compensates for the positive effect of the

DOI:10.1063/1674-0068/26/03/310-320

cobalt electrolyte correlated interfacial energetics, resulting in a less improvement of the voltage by using the cobalt electrolyte compared to the theoretical value.

E. Dependence of photocurrent on the mass transport limitations and charge recombination

It is noteworthy that the iodine-to-cobalt electrolyte alteration has caused a J_{SC} attenuation of about 1 mA for XS39/XS40-sensitized devices. On the other hand, for the XS38- and M12-sensitized devices, the electrolyte alteration has caused significant a J_{SC} reduction of 1.9 and 2.3 mA/cm^2, respectively, leading to decreased PCEs. From the results mentioned above, the sequential negative shift of the E_{CB} are in the order M12<XS38<XS39 for the cobalt cells. Generally, negative shift of E_{CB} leads to a driving force reduction for electron injection as well as an open-circuit photovoltage improvement for DSSCs. Considering the J_{SC} reduction order of M12>XS38>XS39, it can be concluded that the E_{CB} movement is not the main reason for the low J_{SC} of XS38- and M12-sensitized devices employing cobalt electrolyte. Assuming that driving force for electron injection is constant, J_{SC} will be determined by the mass transport and recombination limitations associated with the cobalt redox shuttle, which is varied with different dyes. The origin of the observed J_{SC} trend will be discussed according to these two parameters.

It is known that the mass transport limitation, which results from the larger size of the cobalt complex and greater viscosity of cobalt complex solution, prominently deteriorates the photovoltaic performance of DSSCs employing cobalt electrolytes [39]. To gain insight into the mass transport limitation clearly, photocurrent transients were recorded for cobalt cells under AM 1.5 irradiation (100 mW/cm^2). The photocurrent transients were measured by using an on/off modulation of the incident light. As presented in Fig.9(a), for XS38-, XS39- and M12-sensitized devices, a spike in the photocurrent is observed when the light is switched on, followed by a decrease in photocurrent, eventually reaching a lower stationary value after a few seconds of illumination time. This behavior has been attributed to mass transport limitation of the electrolyte, which limits the photocurrent [40, 41]. This limitation arising from the mass transport is one of the main reasons for the J_{SC} attenuation during iodine-to-cobalt electrolyte alteration.

In addition, a discrepancy in the ratio of the initial peak current to steady state current can be observed between DSSCs sensitized with different dyes. The photocurrent of the XS38 and M12-sensitized devices decreased by around 20% during 0.6 s after light-on. In contrast, the photocurrent of the XS39-sensitized device decreased only by 16%. The discrepancy is more easily distinguished in Fig.9(b), where the current densities

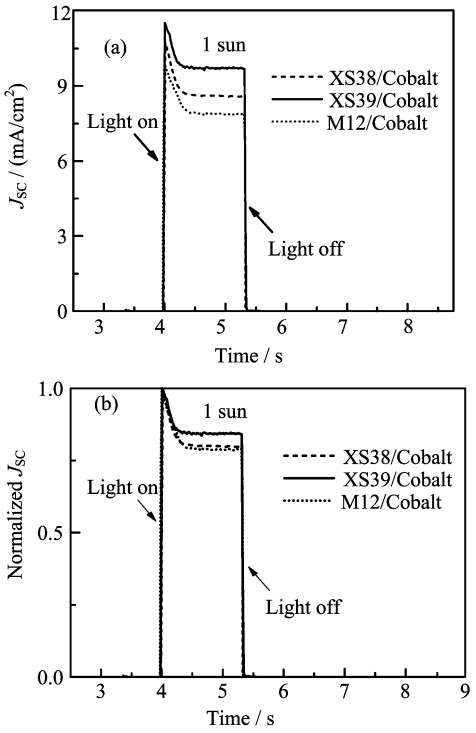

FIG. 9 Photocurrent transients of XS38, XS39 and M12-sensitized devices that utilized the cobalt redox electrolyte (a) without and (b) with normalization of the current density.

are normalized. This indicates that the current depends not only on the slower mass transport of the bulky redox species but also on the recombination of photoinjected electrons with the oxidized form of the redox mediator [13], as discussed above. In other words, the significant J_{SC} reduction for XS38 and M12-sensitized devices can be ascribed to the mass transport limitation of the electrolyte and faster interfacial charge recombination related to XS39-sensitized cobalt cell.

IV. CONCLUSION

In conclusion, four triphenylmaine dyes, XS38, XS39, XS40, and M12, that incorporating combined EDOT and methyl-substituted thieno[3,2-b]thiophene, propyl-substituted thieno[3,2-b]thiophene, methyl-substituted thieno[3,2-b]thiophene and phenylene as the π-conjugated spacers, respectively, were used as organic dyes for DSSCs employing tris(phen)cobalt(II/III) redox shuttle. The results from photovoltaic performance confirm that for XS39 and XS40, the tris(phen)cobalt(II/III) redox couple outperforms the I^-/I_3^- redox couple for thin-film DSSCs. In contrast, M12 and XS38-sensitized devices exhibit better performance when employing iodine electrolyte. EIS measurements show that iodine-to-cobalt electrolyte alteration has caused a different order of charge recombination

DOI:10.1063/1674-0068/26/03/310-320

rate, which is related to the adverse impact of possible halogen bonding, giving an explanation of the opposite V_{OC} variation for the iodine and cobalt cells. Organic dyes with thiophene derivates as linkers are suitable for DSSCs employing cobalt electrolytes. DSSCs sensitized with XS40 in combination with the cobalt redox shuttle yield a DSC with high V_{OC} values reaching 884 mV and an overall power conversion efficiency (PCE) of 6.1% under 100 mW/cm^2 AM1.5 G illumination.

V. ACKNOWLEDGMENTS

This work was supported by the National Natural Science Foundation of China (No.21072152 and No.21101115).

[1] B. O'Regan and M. Grätzel, Nature **353**, 737 (1991).
[2] M. K. Nazeeruddin, P. Péchy, T. Renouard, S. M. Zakeeruddin, R. Humphry-Baker, and M. Grätzel, J. Am. Chem. Soc. **123**, 1613 (2001).
[3] S. Kajiyama, Y. Uemuraa, H. Miura, K. Hara, and N. Koumura, Dyes and Pigments **92**, 1250 (2012).
[4] G. Hagfeldt, L. Boschloo, L. Sun, H. Kloo, and H. Pettersson, Chem. Rev. **110**, 6595 (2010).
[5] Z. Wan, C. Jia, Y. Duan, J. Zhang, Y. Lin, and Y. Shi, Dyes and Pigments **94**, 150 (2012).
[6] Y. Chiba, A. Islam, Y. Watanabe, R. Komiya, N. Koide, and L. Han, Jpn. J. Appl. Phys. Part 2 **45**, L638 (2006).
[7] G. Boschloo and A. Hagfeldt, Acc. Chem. Res. **42**, 1819 (2009).
[8] B.C. O'Regan, I. López-Duarte, M.V. Martínez-Díaz, A. Forneli, J. Albero, A. Morandeira, E. Palomares, T. Torres, and J. R. Durrant, J. Am. Chem. Soc. **130**, 2906 (2008).
[9] T. Marinado, K. Nonomura, J. Nissfolk, M. K. Karlsson, D.P. Hagberg, L. Sun, S. Mori, and A. Hagfeldt, Langmuir **26**, 2592 (2010).
[10] M. Planells, L. Pellejà, J. N. Clifford, M. Pastore, F. De Angelis, N. López, S. R. Marder, and E. Palomares, Energy Environ Sci. **4**, 1820 (2011).
[11] A. Hagfeldt and M. Grätzel, Chem. Rev. **95**, 49 (1995).
[12] H. Nusbaumer, S. M. Zakeeruddin, J. E. Moser, and M. Grätzel, Chem. Eur. J. **9**, 3756 (2003).
[13] S. M. Feldt, E. A. Gibson, E. Gabrielsson, L. Sun, G. Boschloo, and A. Hagfeldt, J. Am. Chem. Soc. **132**, 16714 (2010).
[14] S. M. Feldt, G. Wang, G. Boschloo, and A. Hagfeldt, J. Phys. Chem. C **115**, 21500 (2011).
[15] A. Yella, H.W. Lee, H. N. Tsao, C. Yi, A. K. Chandiran, M. K. Nazeeruddin, E. W. G. Diau, C. Y. Yeh, S. M. Zakeeruddin, and M. Grätzel, Science **334**, 629 (2011).
[16] J. H. Yum, E. Baranoff, F. Kessler, T. Moehl, S. Ahmad, T. Bessho, A. Marchioro, E. Ghadiri, J. E. Moser, C. Yi, M. K. Nazeeruddin, and M. Grätzel, Nat. Commu. **3**, 631 (2012).
[17] Y. Bai, J. Zhang, D. Zhou, Y. Wang, M. Zhang, and P. Wang, J. Am. Chem. Soc. **133**, 11442 (2011).
[18] D. Zhou, Q. Yu, N. Cai, Y. Bai, Y. Wang, and P. Wang, Energy Environ Sci. **4**, 2030 (2011).
[19] J. Liu, J. Zhang, M. Xu, D. Zhou, X. Jing, and P. Wang, Energy Environ Sci. **4**, 3021 (2011).
[20] M. Xu, D. Zhou, N. Cai, J. Liu, R. Li, and P. Wang, Energy Environ. Sci. **4**, 4735, (2011).
[21] Z. H. Wang, M. Liang, L. N. Wang, Y. J. Hao, C. B. Wang, Z. Sun, and S. Xue, Chem. Commun. 5748 (2013).
[22] H. Nusbaumer, J. E. Moser, S. M. Zakeeruddin, M. K. Nazeeruddin, and M. Grätzel, J. Phys. Chem. B **105**, 10461 (2001).
[23] H. X. Wang, P. G. Nicholson, L. Peter, S. M. Zakeeruddin, and M. Grätzel, J. Phys. Chem. C **114**, 14300 (2010).
[24] Y. Liu, J. R. Jennings, Y. Huang, Q. Wang, S. M. Zakeeruddin, and M. Grätzel, J. Phys. Chem. C **115**, 18847 (2011).
[25] H. Han, M. Liang, K. Tang, X. Cheng, X. Zong, Z. Sun, and S. Xue, J. Photochem. Photobiol. A Chem. **225**, 8 (2011).
[26] X. Cheng, M. Liang, S. Sun, Y. Shi, Z. Ma, Z. Sun, and S. Xue, Tetrahedron **68**, 5375 (2012).
[27] S. Ito, T. N. Murakami, P. Comte, P. Liska, C. Grätzel, M. K. Nazeeruddin, and M. Grätzel, Thin Solid Films **516,** 4613 (2008).
[28] S. Wenger, P. A. Bouit, Q. Chen, J. Teuscher, D. Di Censo, R. Humphry-Baker, J. E. Moser, J. L. Delgado, N. Martin, S. M. Zakeeruddin, and M. Grätzel, J. Am. Chem. Soc. **132**, 5164 (2010).
[29] M. Grätzel, J. Photochem. Photobiol. C **4**, 145 (2003).
[30] K. Hara, T. Sato, R. Katoh, A. Furube, Y. Ohga, S. Suga, K. Sayama, H. Sugihara, and H. Arakawa, J. Phys. Chem. B **107**, 597 (2003).
[31] F. Fabregat-Santiago, G. Garcia-Belmonte, J. Bisquert, A. Zaban, and P. Salvador, J. Phys. Chem. B **106**, 334 (2002).
[32] A. Usami, S. Seki, Y. Mita, H. Kobayashi, H. Miyashiro, and N. Terada, Sol. Energy Mater. Sol. Cells **93**, 840 (2009).
[33] X. Hao, M. Liang, X. Cheng, X. Pian, Z. Sun, and S. Xue, Org. Lett. **13**, 5424 (2011).
[34] F. Fabregat-Santiago, J. Bisquert, G. Garcia-Belmonte, G. Boschloo, and A. Hagfeldt, Sol. Energy Mater, Sol, Cells **87**, 117 (2005).
[35] Y. Liang, B. Peng, and J. Chen, J. Phys. Chem. C **114**, 10992 (2010).
[36] M. Lu, M. Liang, H. Han, Z. Sun, and S. Xue, J. Phys. Chem. C **115**, 274 (2011).
[37] T. Privalov, G. Boschloo, A. Hagfeldt, P. H. Svensson, and L. Kloo, J. Phys. Chem. C **113**, 783 (2009).
[38] M. Tuikka, P. Hirva, K. Rissanen, J. Korppi-Tommola, and M. Haukka, Chem. Commun. 4499 (2011).
[39] J. Y. Kim, K. J. Lee, S. H. Kang, J. Shin, and Y. E. Sung, J. Phys. Chem. C **115**, 19979 (2011).
[40] J. J. Nelson, T. J. Amick, and C. M. Elliott, J. Phys. Chem. C **112**, 18255 (2008).
[41] N. Papageorgiou, M. Grätzel, and P. P. Infelta, Sol. Energy Mater. Sol. Cells **44**, 405 (1996).

DOI:10.1063/1674-0068/26/03/310-320